

# Monte Carlo modeling of underwater-image formation: validity of the linear and small-angle approximations

Jules S. Jaffe

A Monte Carlo model has been used to compute a set of point-spread functions (PSF's) and modulation transfer functions (MTF's) that determine underwater-image quality in a range of different environments. The results have been used to analyze the range of application under which a linear-approximation theory holds. Conclusions of the study are that the linear-approximation theory seems to hold quite well over a broad range of applications. The ramifications of the Wells small-angle-scattering theory that predicts the PSF from a knowledge of the volume-scattering function (VSF) are also considered.

Discrepancies are noted between a predicted and a computationally obtained MTF; these discrepancies increase with range. Therefore, the results of the simulations indicate that the small-angle-scattering theory is more valid at a limited number of attenuation lengths. The results of the simulations indicate that the theory is valid to approximately three attenuation lengths.

*Key words:* Ocean optics, Monte Carlo modeling, point-spread function, light scattering.

## 1. Introduction

Although the propagation of light underwater has been an important area of oceanographic research for some time, the practical uses of both theoretical and experimental measurements for the prediction of underwater-image quality is still limited. Previously, I had described the function and capability of a system of computer programs, UNCLES,<sup>1</sup> that model the formation of underwater images. This model was originally developed at the Scripps Institution of Oceanography's Visibility Lab (SIO-Vis Lab) by McGlamery<sup>2</sup> and later extended at the Woods Hole Oceanographic Institution. The output of this system of computer programs is the simulated appearance of an underwater image; the input to the system of computer programs is a characterization of the underwater environment, which includes both the inherent and the apparent properties of the ocean and the arrangement of the cameras, lenses, reflectance map, and lighting sources.

An important piece of information needed to compute realistic images is the modulation transfer function (MTF) of the medium. Various parameteriza-

tions of this function that are subject to different ranges and water conditions are possible. In the most general case, a separate MTF can be considered for each range and each different set of water conditions. Clearly, this makes the job of creation of a computer program to model underwater imaging a very complicated task. On the other hand, if a parametric form of a family of MTF's could be derived that would permit a simple expression to be used it would be of great utility. Toward this goal, several authors have described approximations that employ a small-angle theory. This would seem to be especially valid in consideration of the propagation and scattering of underwater light, as it has been demonstrated experimentally that the phase, or scattering functions, are quite forward peaked.<sup>3,4</sup> In a well-known set of publications, Wells<sup>5,6</sup> showed that, in the small-angle-scattering approximation, a linear relation between the MTF at one range,  $MTF(R_1, \phi)$  could be used to predict the MTF at another range,  $MTF(R_2, \phi)$  by means of

$$MTF(R_1, \phi) = MTF(R_2, \phi)^{R_1/R_2}, \quad (1)$$

where  $\phi$  is the spatial frequency in cycles per radian. This equation is referred to hereafter as the linearity assumption. What it means in simple terms is that the fractional rate of decay of a given frequency component of the MTF is proportional to the distance that the light propagates. In his papers, Wells de-

The author is with the Marine Physical Laboratory, Scripps Institution of Oceanography, La Jolla, California 92093-0238.

Received 2 May 1994; revised manuscript received 7 February 1995.

0003-6935/95/245413-09\$06.00/0.

© 1995 Optical Society of America.

rived a specific form for the MTF that is consistent with the above equation; however, other formulations that are consistent with Eq. (1) are possible. For example, the UNCLES model currently uses a different set of equations that are also consistent with this formulation. Other authors<sup>7</sup> have also solved this problem in a manner consistent with the above.

In addition to the linearity assumption considered above, Wells also considered the potential relation of the MTF, an observed quantity, to an inherent property, the volume-scattering function (VSF). It is quite reasonable to assume that there would be a quantitative relation between these two functions. As such, Wells showed that, given the small-angle-scattering assumption, there was an integral transfer technique which could be used to derive an MTF, or point-spread function (PSF), given a VSF. This relation could also be inverted to compute a VSF, given the PSF. This relation, if it were true in detail, would be extremely valuable. This is because PSF's are fairly easily measured; however the VSF is difficult to measure, especially for the small angles.

Given the attractive features of the above relations, i.e., linearity and the VSF-to-PSF transform, several researchers have evaluated the validity of these techniques in a more rigorous setting. It is widely acknowledged that the best way to simulate a set of outcomes from a given suite of ocean optical experiments is through the use of Monte Carlo computer modeling. These techniques have been well established in the physics community for other applications,<sup>8</sup> and the similarity to this situation permits a straightforward transfer of the methodology. As a consequence of this fact, other authors have applied these modeling techniques to a variety of underwater ocean optical situations.<sup>9-11</sup>

In this regard, McLean<sup>12</sup> examined a comparison of the results of a Monte Carlo model with the predictions of a linear theory that was predicated on the choice of a scattering function whose analytic VSF-PSF transform was known. The conclusion of this study was that the small-angle-scattering theory accounts qualitatively for the radial spread of the downwelling light field with reasonable quantitative agreement for up to 8-10 optical depths. More recently, McLean and Voss<sup>13</sup> published results in which they reported that they had been able to match experimental measurements of the PSF with the same analytic form of the phase function as above for a range of different distances. From their results they conclude that, even if one were to use the incorrect phase function, they could match the experimental data to a relatively high degree. Thus, they conclude that the exact form of the phase function is relatively unimportant for the prediction of the MTF.

In a recent publication, Voss<sup>14</sup> examined the validity of the linearity assumption by analyzing experimental measurements of the PSF at a range of distances under homogeneous ocean-water conditions. The conclusion of this work is that the linearity assumption holds up to ranges of several attenuation lengths.

Study of this subject area has been motivated by the need to have an accurate mathematical and computational model for predicting the performance of underwater-imaging systems. In a previous publication, different classes of underwater-imaging systems were defined together with a qualitative appraisal of their performance capabilities.<sup>1</sup> The development of extended-range underwater-imaging systems has seen considerable activity in recent years. The most modern generation of these underwater-imaging systems relies on sophisticated techniques such as range gating<sup>15</sup> and synchronous scanning.<sup>16</sup> These systems have superior range capabilities when compared with simpler systems that use conventional geometric configurations of cameras and lights. At longer ranges of approximately 3-7 total attenuation lengths, the predictions of the model become more dependent on the degree and the nature of the small-angle scattering. Therefore, accurate knowledge of the image MTF's is highly important.

The study presented in this article is designed to resolve several interesting issues that continue to influence the understanding of the possible simplifications that might be used to model the formation of underwater images. For example, even though the analysis of the linearity assumption presented in both the experimental and the theoretical treatments seems to support its general validity, other interesting issues remain. In particular, when the appearance of an underwater image is simulated, the relative power between the nonzero components of the MTF and the unscattered beam is extremely important. This issue has not been treated owing to a lack of experimental data.<sup>14</sup> Also, even though the MTF data has been fitted by means of data analysis, the exact form of the VSF was not known at the time. Therefore, the validity of the transform of MTF to VSF is still an open issue. In fact, it is unlikely that a general statement with regard to this relation can be made because the validity of the transformation depends strongly on the shape of the VSF function. Therefore I decided to use a set of test data of a measured VSF<sup>4</sup> in conjunction with a Monte Carlo model to examine the validity of these issues in the context of this specific, measured function.

## 2. Description of the Numerical Techniques

As stated in Section 1, a Monte Carlo simulation model was created to examine the answers to the questions posed. The mathematical and statistical assumptions inherent in this procedure are well known in the literature<sup>8,17</sup> and are not covered in depth in this article. The basic geometry of the situation is outlined in Fig. 1. Here, it can be seen that a single experimental simulation consists of launching some number of photons toward the surface of a sphere of radius  $R$  and collecting the data that describe the radiance at each point on its surface. If the source can be considered to be a point source, it can then be described by the radiant energy that is projects as a function of angles  $\theta$  and  $\phi$  onto the surface of a sphere at distance  $R$ ,  $L(\theta, \phi, R)$ . Here,  $\theta$

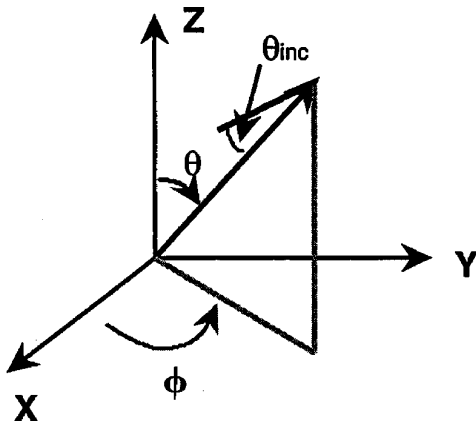


Fig. 1. Coordinate system for the Monte Carlo simulation.

and  $\phi$  are the angles consistent with a spherical coordinate system as illustrated in Fig. 1. Also shown in the figure is the angle incident upon the surface of the sphere,  $\theta_{inc}$ .

One common assumption is that the scattering from a surface can be assumed to follow a Lambertian distribution. In this case the MTF can be derived through the creation of an omnidirectional point source and the computation of the radiant distribution that is due to the source at the entrance to an imaging device. In this regard, the simplest type of device that can be imagined is a pinhole camera. Then, the radially symmetric radiant distribution at the location of the entrance to the pinhole camera is exactly the PSF. A straightforward Hankel transform of this function will then produce the MTF.

Although there are many types of simulations that could be used to determine the incident radiance on the surface of a sphere for an omnidirectional source, the technique used here was designed to expedite the numerical speed at which the simulations could be executed. In this regard, note that if the photons could simply be launched along the  $z$  axis instead of omnidirectionally, then a few numerical operations could be saved with respect to computer-execution time. It is now demonstrated how this can be made possible.

First note that, for the omnidirectional source, the radiance incident on the surface of a sphere of arbitrary diameter is the same at each and every point, and, moreover, it is cylindrically symmetric, i.e.,  $L(\theta, \phi, \theta_{inc}, \phi_{inc}) = L(\theta_{inc})$ . Here,  $\theta_{inc}$  and  $\phi_{inc}$  are the incident angles on the surface of the sphere and  $\theta$  and  $\phi$  define the location of the point on the surface of the sphere in a spherical coordinate system. Next, note that the radiance that is due to an omnidirectional source can be derived from the unidirectional source if one convolves the latter with a function that is a constant regardless of direction, i.e., an omnidirectional constant. Let  $L_O(\mathbf{R}, \xi)$  be the radiance that is incident on a point on the surface of the sphere and that is due to the omnidirectional source and let  $L_u(\mathbf{R}, \xi)$  be the radiance distribution for a unidirectional light source that is aimed along the  $z$  axis.

Then, by means of the principle of superposition,

$$L_O(\mathbf{R}, \xi) = \int C(\xi') L_u(\mathbf{R}, \xi - \xi') d\Omega', \quad (2)$$

where  $C(\xi')$  is a constant that is independent of angle and  $d\Omega'$  is a weighting function that depends on the solid angle. The physical realization of this equation can be accomplished if one simply points the unidirectional source into all given directions and integrates the results. In addition, this equation can be parameterized any way we like. For example, let us assume  $L_u(\mathbf{R}, \xi - \xi')$  to be a piecewise continuous function in little solid angular regions of  $N$  equal areas,  $\Delta\Omega'$ , then we can write  $L_O(\mathbf{R}, \xi) = \Delta\Omega' / 4\pi \sum_{i=1}^N L_{ui}(\mathbf{R}, \xi')$ . Note that the division by  $4\pi$  ensures that the total number of photons in the unidirectional beam is equal to the number of photons in the omnidirectional situation (as  $\sum_{i=1}^N \Delta\Omega' / 4\pi = 1$ ). Alternatively, parameterizing this equation in  $\theta$  and  $\phi$  i.e., spherical coordinates, and assuming a piecewise continuity of the function in between the values  $\theta_0, \theta_1, \dots, \theta_N$ , implies that

$$\begin{aligned} L_O(\mathbf{R}, \xi) &= \frac{1}{4\pi} \int L_{ui}(\theta, \phi, \theta_{inc}, \phi_{inc}) \sin \theta d\theta d\phi \\ &= \sum_{i=0}^{N-1} L_{ui}(\theta_i, \theta_{inc}, \phi_{inc}) \frac{(\cos \theta_i - \cos \theta_{i+1})}{2}, \end{aligned} \quad (3)$$

where  $\theta_0 = 0$ . Now, let us assume that  $p_n(\theta_i, \theta_{inc}, \phi_{inc})$  is the number of photons incident at a given point on the interior of the sphere, in an annulus of the solid angle  $\Delta\Omega(i)_{inc}$ , an estimator of  $L_{ui}(\theta, \phi, \theta_{inc}, \phi_{inc})$  is

$$\frac{p_n(\theta_i, \theta_{inc}, \phi_{inc})}{2\pi R^2 \cos \theta_{inc}' (\cos \theta_i - \cos \theta_{i+1}) \Delta\Omega(i)_{inc}}, \quad (4)$$

where  $\theta_{inc}'$  is an angle halfway between  $\theta_i$  and  $\theta_{i+1}$ , so that

$$L_O(\mathbf{R}, \xi) = \sum_{i=0}^{N-1} \frac{p_n(\theta_i, \theta_{inc}, \phi_{inc})}{\cos \theta_{inc}' \Delta\Omega(i)_{inc} 4\pi R^2}. \quad (5)$$

Now, to compute the number of photons per unit solid angle of incidence, let us assume that the  $p_n$  function is piecewise continuous in between the incidence angles,  $\theta(0)_{inc}, \theta(1)_{inc}, \dots, \theta(N)_{inc}$ , and because  $\delta\theta = 2\pi[\cos \theta(i)_{inc} - \cos \theta(i+1)_{inc}]$  compute

$$\begin{aligned} L_O(\theta_{inc}') &= \\ &= \sum_{i=1}^{N-1} \frac{p_n(\theta_i, \Delta\theta_{inc}')}{8\pi^2 R^2 \cos(\theta_{inc}') (\cos \theta(i)_{inc} - \cos \theta(i+1)_{inc})}, \end{aligned} \quad (6)$$

where  $p_n(\theta_i, \Delta\theta_{inc}')$  is the number of photons that fall into the bin between  $\theta(i)_{inc}$  and  $\theta(i+1)_{inc}$  and  $\theta_{inc}'$  is an angle halfway between  $\theta_i$  and  $\theta_{i+1}$ . This formula states that it is simply necessary to bin the number of

photons that strike the sphere as a function of incidence angle and then to normalize by dividing by the solid angle subtended by that annulus and the cosine of the incidence angle to obtain an estimate of the PSF. This is the procedure that was used to compute the PSF for the omnidirectional source.

In the simulation, photons of unit value are first launched along the  $z$  axis. Then, a random number is generated from a scattering-distribution function that describes the probability of a photon scattering per unit length. Let  $\theta$  and  $\phi$  be the spherical-coordinate angles that are relative to the current photon trajectory. Once a photon is scattered, the new direction in  $\phi$  is chosen at random between 0 and  $2\pi$ , and the new direction in  $\theta$  is chosen through the use of the VSF as the probability density function as  $\beta(\theta)\sin(\theta)$ . As an aid to the computational speed, the data for the VSF is precalculated and stored in lookup tables. Photons are also attenuated over their propagation distance by the absorption coefficient. This process is continued until the photon strikes the surface of the sphere. The approximate error bounds for the data were estimated when the program was run a number of times (10) with different sets of random numbers and the consistency examined between runs. Assuming that the variability between both data points of the PSF and that the variability between runs each were uncorrelated yielded an estimate of approximately several percent in the uncertainty of the computed MTF functions.

Final values were obtained from  $10^7$  photons/simulation. Because this number of photons contributed to only 1025 angular bins ( $0 \leq \theta \leq \pi/2$ ) for the PSF, the degree of overdetermination of the data was high. Normal times to complete a given set of computer runs for a given set of water conditions were of the order of 1–4 hours (computed on a Sun Sparcstation 2).

The data were analyzed in several ways. A program was written to perform the Hankel transform of the PSF data to obtain the MTF through the use of the projection-slice theorem.<sup>18</sup> Several sets of test data whose analytic Handel transforms are known were used to ensure the correctness of this procedure

The validity of the Wells PSF-to-VSF transform was judged through the use of an additional computer program that was written. Wells describes two techniques for computing the transform.<sup>6</sup> One of these techniques was considered to be more numerically stable. The technique used was first to compute the Hankel transform of the data and then to resample and to integrate the data. These transforms are also discussed in Ref. 13. Given the volume scattering function,  $\beta(\theta)$ , one computes

$$\Sigma(\phi) = \int_0^\pi J_0(2\pi\phi\theta)\beta(\theta)\theta d\theta. \quad (7)$$

Resampling this transform by defining a function  $Q$ ,

$$Q_W(\phi) = \int_0^1 \Sigma(\phi t) dt, \quad (8)$$

permits Wells' complete expression for the MTF to be computed as

$$\text{MTF}_W(\phi) = \exp[Q_W(\phi) - s_t]R. \quad (9)$$

Here,  $R$  is the range from the source to the location where the MTF or the PSF is being measured, and  $\phi$  is the angular frequency in cycles per radian. Wells states that  $s_t$  can be computed by integrating the VSF as

$$s_t = 2\pi \int_0^{\Theta_{\max}} \beta(\theta)\sin(\theta)d\theta. \quad (10)$$

Here,  $\Theta_{\max}$  is some suitable value of  $\theta$  chosen so that almost all the power is contained in the values from 0 to  $\Theta_{\max}$ . It is interesting to note (as does Wells<sup>5</sup>) that in the limit of  $\phi \rightarrow \infty$ ,  $Q_W(\phi) \rightarrow 0$  and therefore  $\text{MTF}_W(\infty) = \exp(-s_t R)$ . Thus, this value can be viewed as a constant offset in Fourier space whose inverse transform is a  $\delta$  function in the spatial domain. In this interpretation  $s_t$  can therefore be viewed as an *effective* beam-attenuation coefficient that includes the results of small-angle scattering but does not remove enough radiant energy to appear in the  $Q_W(\phi)$  component.

The numerical implementation of this algorithm was checked through the use of functions whose analytic transformations are known. For example, Wells<sup>6</sup> describes the fact that, if

$$\beta(\theta) = \frac{\theta_0}{2\pi(\theta_0^3 + \theta^3)^{3/2}}, \quad (11)$$

then

$$Q_W(\phi) = \frac{1 - \exp(-2\pi\theta_0\phi)}{2\pi\theta_0\phi}. \quad (12)$$

Extremely close agreement (<1%) was obtained for values ( $\theta_0 = 0.03$ ) that have been indicated to yield a good fit to the obtained PSF's.<sup>13</sup>

### 3. Results

Through the use of the above numerical suite of programs, a set of different simulations was performed to compare the various issues of both linearity and the Wells PSF-to-VSF transform. Table 1 contains the values of the inherent ocean optical proper-

Table 1. Inherent Ocean Optical Parameters Used in the Simulations

Water Type	Coefficients ( $\text{m}^{-1}$ )		
	Absorption $a$	Total Scattering $b$	Total Absorption $c$
Bay	0.143	0.18	0.323
Coastal	0.041	0.211	0.252
Deep ocean	0.019	0.03	0.049

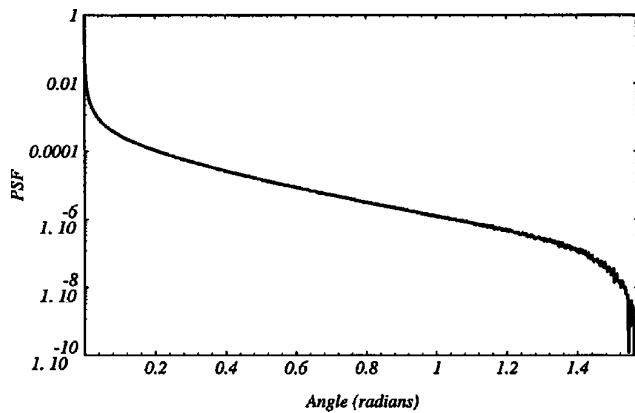


Fig. 2. PSF output after  $10^7$  photons at 6 attenuation lengths in bay water.

ties that were used for the simulations. These were taken from a U.S. Navy handbook of underwater imaging<sup>20</sup> as being indicative of different typical environments: bay, coastal, and deep-oceanic conditions. In all cases, one of Petzold's measured VSF's (Autec, Test 161, Station 8) was used. This is widely considered to be one of the best available data sets.<sup>4</sup> Additional indications that this function is invariant in different oceanic conditions are contained in Ref. 20. One problem that occurs when this function is used is that, because no value was obtained for the VSF at zero degrees, a suitable approximation needed to be made. The approach taken here was to simply use the value for the smallest scattering value that was obtained as the value for the unscattered beam as well. Although other approaches were clearly possible, such as interpolation of the zero value with different functions, this smallest-obtained-value approach was used as a reasonable method to obtain this value. Twelve sets of simulations were done: The range of 1, 3, 6, and 10 total attenuation lengths (c) was carried out for each of the three environments mentioned above.

The data sets obtained were analyzed through several techniques. Figure 2 shows a graph of one of the PSF's obtained. Here we graph  $PSF(\theta)$  of the output data. As evidenced in the graph, the noise does not seem to dominate until approximately quite a high angle. Figures 3(a)–3(c) show the logarithm of the values of the MTF's as functions of the angle. The MTF's themselves were obtained by means of a Hankel transform of the PSF data. The figure illustrates that, qualitatively, the data follow the expected trend: that is, the larger distances result in both a lower asymptotic value as well as a steeper slope. A more detailed analysis was performed to compare the MTF's through the determination of ratios, as in

$$LN(R_1 R_2) = \frac{\ln[MTF(\phi, R_1)]}{\ln[MTF(\phi, R_2)]}. \quad (13)$$

Given the predictions of the linear theory, these ratios should be equal to the ratios of the different

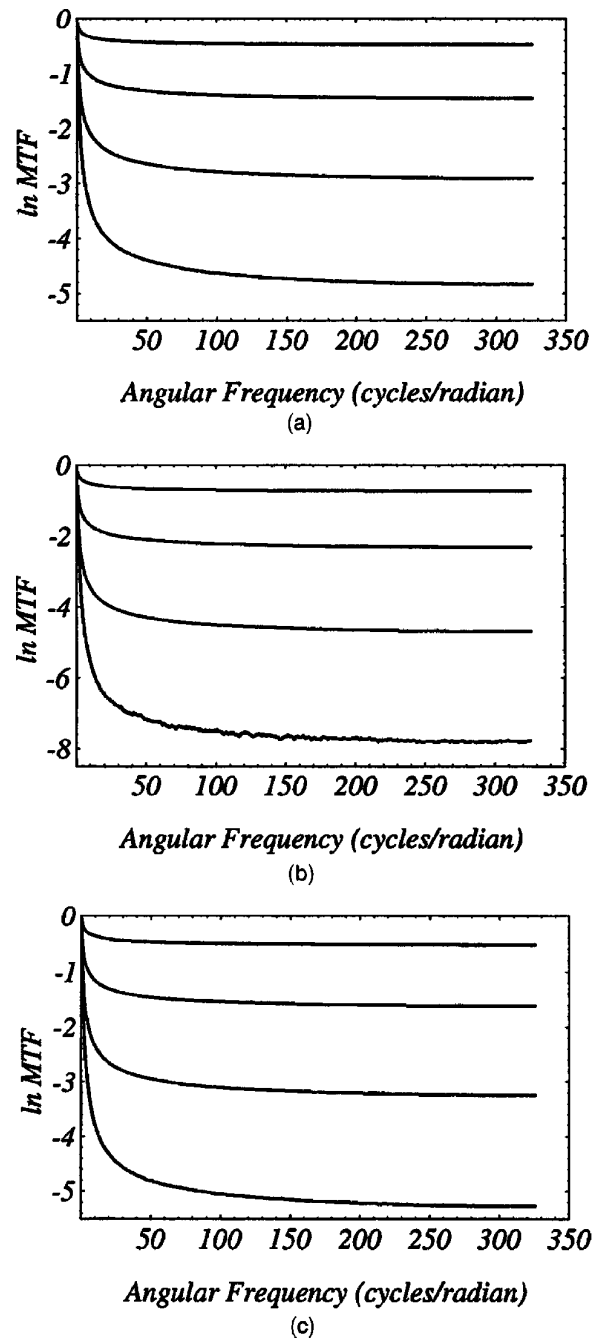
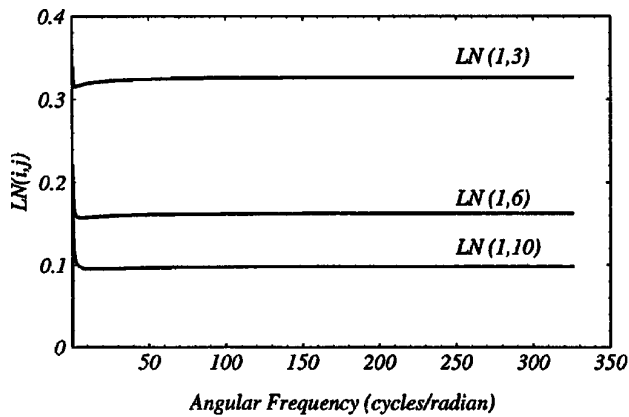


Fig. 3. Logarithms of the values of the MTF's for (a) bay waters, (b) coastal waters, and (c) deep-oceanic waters.

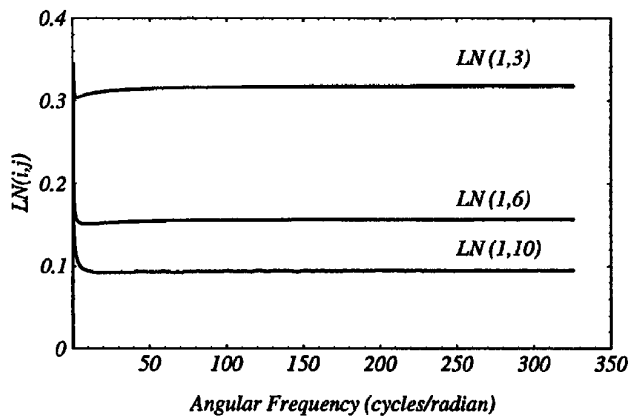
ranges, i.e.,

$$LN(R_1 R_2) = \frac{\ln[\exp[Q(\phi) - s_l R_1]]}{\ln[\exp[Q(\phi) - s_l R_2]]} = \frac{R_1}{R_2}. \quad (14)$$

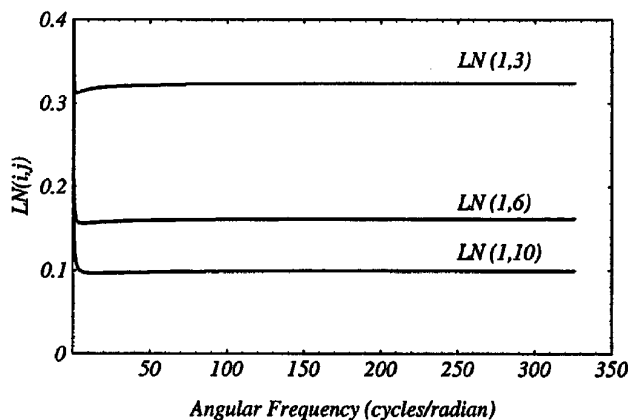
These values are shown in Fig. 4. As can be seen from the plots, the data seem to obey the predictions of the linear theory quite well. For example, when the MTF is used at 1 attenuation length, the value of the MTF at 10 attenuation lengths is predicted to within 2%. Although discrepancies are noted at low spatial frequencies, it appears that if the MTF is used



(a)



(b)



(c)

Fig. 4. Values for the  $LN_{R_1, R_2}$  functions (see text) for (a) bay waters, (b) coastal waters, and (c) deep-ocean waters.

at small numbers of attenuation close to the origin, the MTF can be predicted at longer ranges.

In addition, the  $Q$  functions were compared across water types and also with the function derived above from the Wells algorithm. Figure 5 shows the set of  $Q$  functions obtained at 6 total attenuation lengths for the three different water types. In addition, the Wells  $Q$  function (dashed curve) is displayed. The graph indicates that the  $Q$  function obtained from the Wells theory predicts the shape of the measured  $Q$  function extremely well at low spatial frequencies; however, substantial discrepancies are noted at high

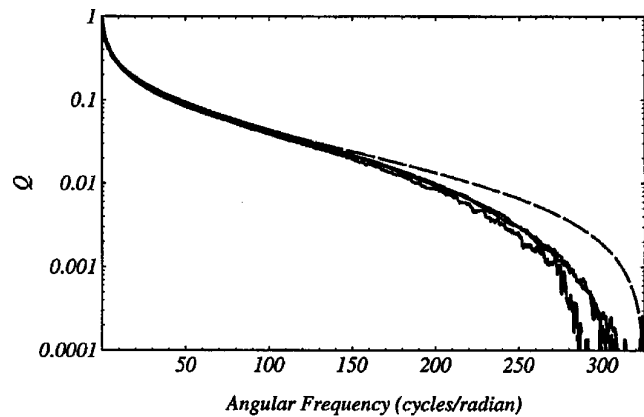


Fig. 5. Comparison of the  $Q$  functions across water types at 6 attenuation lengths (solid curves) with the Wells theory (dashed curve).

spatial wave numbers. The  $Q$  function derived from the Wells theory therefore predicts that there will be a greater transfer of high-frequency information in the MTF than the Monte Carlo simulations indicate. This, in turn, leads to a narrower PSF for the Wells theory than that predicted from the Monte Carlo simulations, as is evidenced in the following discussion.

The comparison of the MTF's predicted by means of the Wells theory versus the results of the Monte Carlo program were completed through the use of the  $Q$  functions, derived above in expression (7), to compute the MTF's. Then, an inverse Hankel transform was taken to compute the PSF's. Figure 6 illustrates a comparison of the results of the computations. As a numerical note, when the inverse Hankel transforms of the computed MTF's were taken, some oscillatory behavior was noticed, especially for the shorter attenuation lengths for which the MTF was still substantial at higher spatial frequencies. For stabilization of the transform, the value of the MTF at the highest spatial frequency was subtracted from all the values before the inverse Hankel transform was taken. In the spatial-frequency domain, this corresponds to subtracting a constant value from all of the data. In the spatial domain, this corresponds to the subtraction of a delta function at the origin from the data. The plots shown in Fig. 6 are the inverse Hankel transforms, constrained to asymptote to zero in the frequency domain for both the Wells simulated and the Monte Carlo data. Thus, the delta function at the origin has not been added back into the data. In the case of the Wells data, the asymptotic value of the Hankel transform of the Monte Carlo data was used to estimate a value for each range and water type for  $s_i R$ , as above. Because  $Q(\phi) \rightarrow 0$  as  $\phi \rightarrow \infty$ , the last computed value of the MTF should provide a reasonable value of  $s_i R$ . This last value was then subtracted from the frequency-domain data before inverse Hankel transformation. Thus, the figure shows a graph of

$$\text{MTF}_{W_i}(\phi) = \exp[Q(\phi) - s_i R] - \exp(-s_i R), \quad (15)$$

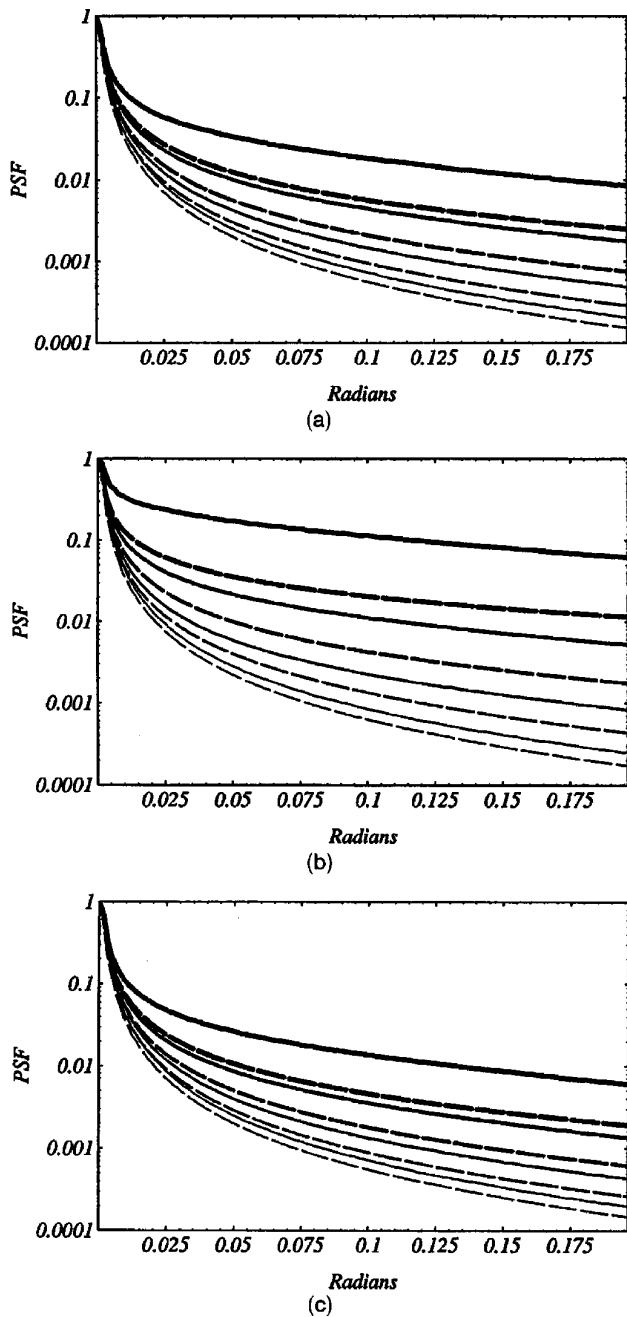


Fig. 6. A comparison of the PSF's for the four attenuation-length ranges and three water types: Simulations for (a) bay, (b) coastal, and (c) deep-ocean water are shown for 1, 3, 6, and 10 attenuation lengths. The results of the Monte Carlo simulations (solid curves) are shown along with the predictions of the Wells theory (dashed curves). The thickness of a curve indicates its attenuation length, with 1 attenuation length the thinnest and 10 attenuation lengths the thickest curves.

for the Wells-computed inverse Hankel transforms versus the Monte Carlo data with the same numerical value subtracted from the frequency-space data. Minor discrepancies at 1 total attenuation length can be observed, and these discrepancies grow larger as the total number of attenuation lengths is increased. This indicates that, for the Petzold PSF (with our

interpolation scheme for the unscattered beam), the Wells transform becomes less accurate as the total number of attenuation lengths is increased.

#### 4. Discussion

The basic goal of the research described in this article has been to examine the validity of several simplifying assumptions that have been proposed to model the propagation of light underwater. The technique used has been to compare the results of a Monte Carlo model to results obtained from the set of approximations. In one case the linearity assumption has been tested, and it has been found that this approximation is valid to the range of 10 attenuation lengths with some discrepancies noted at small spatial frequencies.

In addition, the data have been used to examine the validity of the Wells transform, which permits the derivation of the PSF from the VSF or vice versa. In this case, let us note a discrepancy between the function predicted from the Wells theory and the function derived by means of the Monte Carlo simulation. In particular, the Wells theory predicts, at medium to large numbers of attenuation lengths, a substantially less-spread beam than that predicted by the Monte Carlo simulation. An interesting question arises as to why the small-angle-scattering theory seems to break down at larger numbers of attenuation lengths. In speculating why this is so, we note that the Wells theory, as stated already, computes a PSF at a small number of attenuation lengths under the assumption of a small-angle approximation. Then, the PSF at longer attenuation lengths is derived from that one by means of a range-dependent multiplication in Fourier space, or, equivalently, an autoconvolution in the spatial domain. These simulations indicate that this autoconvolution operation underestimates the true amount of scatter for the Petzold VSF as used here. Whether this error is more or less for other candidate VSF functions is currently an open question.

In comparing these results with previous ones it is important that one notes that the experiments done by Voss<sup>14</sup> used a Lambertian point source, which has a cosine distribution. Because our simulations have been executed by simulation of an omnidirectional source, the question arises as to whether there is a substantial difference between the two. That is, is it really valid to compare the PSF's obtained (by means of simulations) with an omnidirectional source with those obtained (experimentally) with a cosine source? To explore the answer to this question I used the equivalence between the beam-spread function and the PSF.<sup>21,22</sup> Here, let us note that the beam-spread function associated with a cosine receiver can be equated to the PSF associated with a cosine source. As such, the computer program was used in a mode that permitted the vector irradiance to be measured on the surface of the sphere as a function of position. Here, we use the same method that was described by Kirk<sup>23</sup> to compute the vector irradiance. That is, simply sum up the number of photons crossing the surface at the specific set of positions within the

angular bin. However, Eq. (4) was then applied to normalize for the differences in surface area within the annulus. The bay-water case was executed with  $10^7$  photons at 1, 3, 6, and 10 total attenuation lengths. The result of this procedure revealed that there was indeed a very small difference ( $<0.5\%$  only at 10 attenuation lengths) in the PSF's between the cosine source and the omnidirectional source. This is not surprising, as the extreme forward peak of the VSF occurs in a region over which the cosine function changes little. On the other hand, computational verification provides a necessary check of this assumption.

It is interesting to compare our simulations with other results. For example, Voss<sup>14</sup> demonstrates that data collected in the Sargasso Sea seem to obey the linearity relation quite well, as we note here. With respect to the VSF-to-PSF transform, to my knowledge no one has ever published results of having applied the Well's transform to Petzold's data and then compared it to the results of a Monte Carlo simulation. As an analytic expression for this data does not exist, apparently the only way to accomplish this is by means of the numerical technique, as explained above. On the other hand, McLean et al.<sup>12</sup> have taken the expression in Eq. (6) and used it as a VSF in a Monte Carlo model to derive a set of MTF's. They have compared that VSF with the analytic result of Eq. (7).

An interesting feature of our choice of  $s(a, b, R)$  is that it results in the smoothest function for  $Q(\phi)$ . This is intuitively appealing because it results in a smooth interpolation of the PSF at the origin value. The reason this choice results in the smoothest function is that it minimizes the high-frequency content of the power spectrum of the PSF. For example, assume that the PSF consists of the sum of two parts, an unscattered, or constant, component and another function that consists of the remainder of the PSF. Then

$$\text{PSF}_{\text{total}} = \text{PSF}_{\text{unscat}} + \text{PSF}_{\text{scat}} \quad (16)$$

This function will have a discontinuity at the origin because of the unscattered component. What is the most natural way, then, to apportion the energy in the MTF at 0 cycles/rad to the unscattered component and the scattered one? One technique is to interpolate the scattered PSF smoothly to the value at the origin. This is automatically accomplished if the MTF is decomposed into two components, so that the asymptotic value of the  $\text{MTF}_{\text{scat}}$  is 0. This is because the MTF is a monotonically decreasing function. From the linearity of the Hankel transform:

$$\text{MTF}_{\text{total}} = \text{MTF}_{\text{unscat}} + \text{MTF}_{\text{scat}} \quad (17)$$

Because the Fourier transform of a  $\delta$  function is a constant, the  $\text{MTF}_{\text{total}}$  can be regarded as the sum of a constant  $K$  plus some other function:

$$\text{MTF}_{\text{total}} = K + \text{MTF}_{\text{scat}} \quad (18)$$

Setting the asymptotic part of the  $\text{MTF}_{\text{scat}}$  to zero minimizes the amount of power in the high-frequency part of this function. On the basis of this analysis, it is conjectured that the choice of the decomposition that causes the MTF of the scattered component to approach 0 results in the smoothest choice for the MTF of the scattered radiation. However, this treatment does not guarantee that the function obtained for  $\text{MTV}_{\text{unscat}}$  does not include some radiation that has been scattered at extremely small angles. In fact, it might be possible that the values obtained for these two parameters at the origin are a function of the angular resolution of either the numerical implementation or of the experimental measurement. In this case, the results would be dependent on the implementation. In this simulation, 1025 angular bins were used for the PSF, and this results in a resolution in angle of approximately 1.5 mr. This value is comparable to the resolution obtained with experimental measurements of the PSF.

In conclusion, it appears that several simplifications are indeed possible when one models the propagation of light underwater. In particular, with this analysis, the appropriate function  $Q_M(\phi)$  can be used to compute the PSF and MTF for a fairly wide distribution of water types and over a fairly wide distribution of distances, when combined with a set of empirical beam-attenuation constants (one for each water type). It also seems likely that this function depends primarily on the VSF, as the VSF is approximately the same for all of the simulations in our study. This circumstance is encouraging because it may be possible, with future methods, to compute the MTF from the VSF. Unfortunately, at the present time the only way that I am aware of that yields a valid function for large numbers of attenuation lengths across a variety of VSF's is through the use of the type of Monte Carlo simulation accomplished in this study. Presumably this limitation is not a problem, as it needs only to be done once per VSF.

This work was supported by the Office of Naval Research under grant N0014-89-J-1419. The author also thanks K. Voss and H. Gordon for helpful criticism of the manuscript.

## References

1. J. S. Jaffe, "Computer modeling and the design of optimal underwater imaging systems," *IEEE J. Ocean Eng.* **15**, 101-111 (1990).
2. B. J. McGlamery, "A computer model for underwater camera systems," in *Ocean Optics VI*, S. Q. Duntley, ed., Proc. Soc. Photo-Opt. Instrum. Eng. **208**, 221-231 (1979).
3. N. G. Jerlov, *Marine Optics*, Vol. 14 of *Elvesier Oceanography Series* (Elvesier, New York, 1976).
4. T. J. Petzold, *Volume Scattering Functions for Selected Ocean Waters* (Scripps Institution of Oceanography, La Jolla, Calif., 1972), pp. 72-78.
5. W. H. Wells, "Loss of resolution in water as a result of multiple small-angle scattering," *J. Opt. Soc. Am.* **59**, 686-691 (1969).
6. W. H. Wells, "Theory of small-angle scattering," *AGARD Lect. Ser.* **61**, 1-19 (1973).
7. D. Arnush, "Underwater light-beam propagation in the small-

- angle-scattering approximation," *J. Opt. Soc. Am.* **62**, 1109–1111 (1972).
8. E. E. Lewis and W. F. Miller, Jr., *Computational Methods of Neutron Transport* (Wiley, New York, 1984).
  9. G. W. Kattawar and C. N. Adams, "Stokes vector calculations of the submarine light field in an atmosphere-ocean with scattering according to a Rayleigh phase matrix: effect of interface refractive index on radiance and polarization," *Limnol. Oceanogr.* **34**, 1453–1472 (1989).
  10. R. H. Gordon, "Ship perturbation of irradiance measurements at sea. 1: Monte Carlo simulations," *Appl. Opt.* **24**, 4172–4182 (1985).
  11. J. T. O. Kirk, "The upwelling light stream in natural water," *Limnol. Oceanogr.* **34**, 1410–1425 (1989).
  12. J. W. McLean, D. R. Crawford, and C. L. Hindman, "Limits of small-angle scattering theory," *Appl. Opt.* **26**, 2053–2054 (1987).
  13. J. W. McLean and K. J. Voss, "Point-spread function in ocean water: comparison between theory and experiment," *Appl. Opt.* **30**, 2027–2030 (1991).
  14. K. J. Voss, "Variation of the point-spread function in the Sargasso Sea," in *Underwater Image, Photography, and Visibility*, R. W. Spinrad, ed., *Proc. Soc. Photo-Opt. Instrum. Eng.* **1537**, 97–103 (1991).
  15. B. Swartz and J. D. Cummings, "Laser range-gated underwater imaging including polarization discrimination," in *Underwater Imaging, Photography, and Visibility*, R. W. Spinrad, ed., *Proc. Soc. Photo-Opt. Instrum. Eng.* **1537**, 42–56 (1991).
  16. T. J. Kulp, D. Garvis, R. Kennedy, and T. Salmon, "Results of the second tank trial of the LLNL/NAVSEA underwater laser imaging system," in *Ocean Optics X*, R. W. Spinrad, ed., *Proc. Soc. Photo-Opt. Instrum. Eng.* **1302**, 398–413 (1990).
  17. J. Arvo and D. Kirk, "Particle transport and image synthesis," *Comput. Graphics* **24**, 63–66 (1990).
  18. A. V. Oppenheim, G. Frisk, and D. R. Marinez, "Computation of the Hankel transform using projections," *J. Acoust. Soc. Am.* **68**, 523–529 (1980).
  19. C. J. Funk, S. B. Bryant, and P. J. Heckman, Jr., *Handbook of Underwater Imaging System Design* (Ocean Technology Department, Naval Undersea Center, San Diego, Calif., 1972).
  20. L. E. Mertens and F. S. Replogle, Jr., "Use of point-spread and beam-spread functions for analysis of imaging systems in water," *J. Opt. Soc. Am.* **67**, 1105–1117 (1977).
  21. J. Tyler, "Optical properties of water," in *Handbook of Optics*, W. G. Driscoll and W. Vaughan, eds. (McGraw-Hill, New York, 1978), pp. 15.1–15.38.
  22. H. R. Gordon, "Equivalence of the point- and beam-spread functions of scattering media—a formal demonstration," *Appl. Opt.* **33**, 1120–1122 (1994).
  23. J. T. O. Kirk, "Monte Carlo procedure for simulating the penetration of light into natural waters," CSIRO Paper 36 (Commonwealth Scientific and Industrial Research Organization, Division of Plant and Industrial Technology, Canberra, Australia, 1981), pp. 1–16.